ACS APPLIED MATERIALS & INTERFACES

Research Article

www.acsami.org

Highly Efficient Removal of Pathogenic Bacteria with Magnetic Graphene Composite

Sihui Zhan,*[,†] Dandan Zhu,[†] Shuanglong Ma,[†] Wenchao Yu,[†] Yanan Jia,[†] Yi Li,[§] Hongbing Yu,[†] and Zhiqiang Shen*[,∥]

[†]College of Environmental Science and Engineering, Key Laboratory of Environmental Pollution Process and Environmental Criteria, Nankai University, Tianjin 300071, P. R. China

[§]Department of Chemistry, Tianjin University, Tianjin 300072, P. R. China

[∥]Institute of Health and Environmental Medicine, Tianjin 300050, P.R. China

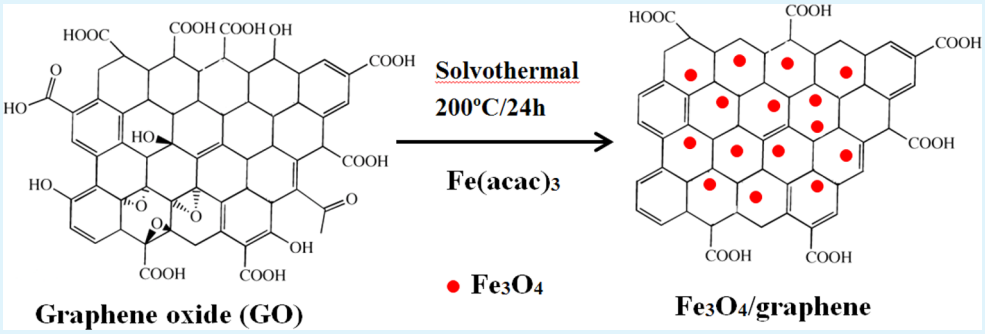

ABSTRACT: Magnetic Fe_3O_4/graphene composite (abbreviated as G-Fe_3O_4) was synthesized successfully by solvothermal method to effectively remove both bacteriophage and bacteria in water, which was tested by HRTEM, XRD, BET, XPS, FTIR, CV, magnetic property and zeta-potential measurements. Based on the result of HRTEM, the single-sheet structure of graphene oxide and the monodisperse Fe_3O_4 nanoparticles on the surface of graphene can be observed obviously. The G-Fe_3O_4 composite were attractive for removing a wide range of pathogens including not only *bacteriophage ms2*, but also various bacteria such as *S. aureus*, *E. coli*, *Salmonella*, *E. Faecium*, *E. faecalis*, and *Shigella*. The removal efficiency of *E. coli* for G-Fe_3O_4 composite can achieve 93.09%, whereas it is only 54.97% with pure Fe_3O_4 nanoparticles. Moreover, a detailed verification test of real water samples was conducted and the removal efficiency of bacteria in real water samples with G-Fe_3O_4 composite can also reach 94.8%.

KEYWORDS: *graphene, magnetic nanoparticles, pathogenic bacteria*

1. INTRODUCTION

It is reported that more than 1.3 million deaths of children was caused by diarrheal illness worldwide every year.[1,2] One of the transmission routes is unclean water contaminated with pathogens bacteria. Thus, the safety of drinking water is attracting more considerable attention around the world. Furthermore, among of the fecal coliform bacteria count, *Escherichia coli* (*E. coli*), is most commonly used as fecal indicator bacteria for water quality monitoring and water safety management, which can result in diarrhea, hemorrhagic colitis, and hemolytic uremic syndrome.[3−5] Because of the pathogens, bacteria can still stay in the environment for a long time and resist common disinfection methods.[6] Therefore, there is a critical need to develop new technologies that can clean bacteria and viruses from water simultaneously and conveniently.

Among the various techniques used to remove bio-organic pollutants in water, such as physical processes (adsorption, distillation, and filtration),[7,8] biological processes (activated sludge), chemical processes (flocculation and chlorination),[9,10] and photocatalytic process,[11] the application of nanomaterials in water has been extensively studied because of its small size effect, quantum size effect, huge surface effect, good mechanical properties, and so on in recent years.[12] However, because of its small size, it is difficult to separate nanomaterials from water, which not only resulted in difficulty to recycle and reuse nanomaterials but also may generate serious secondary pollutions. To overcome these problems, a kind of novel magnetic nanomaterials was developed recently, which can be easily separated from water with an external magnet.[13,14] However, the removal efficiency of pathogen bacteria through only magnetic nanomaterials is very low, and these pure magnetic nanomaterials usually agglomerate easily. Thus, it has aroused many scientists' great interest to develop novel functionalized magnetic nanomaterials that not only show higher removal efficiency of pathogens bacteria but also can be easily separated from water.

Received: December 9, 2014
Accepted: January 29, 2015
Published: January 29, 2015

DOI: 10.1021/am508682s
ACS Appl. Mater. Interfaces 2015, 7, 4290−4298

Scheme 1. Synthesis Route of G-Fe_3O_4

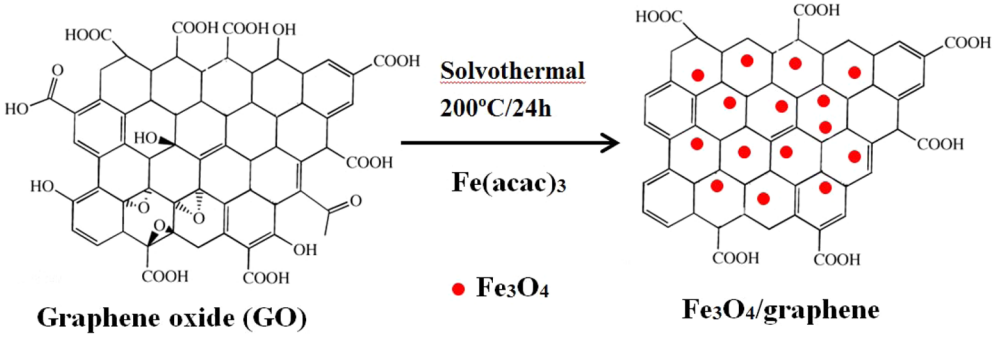

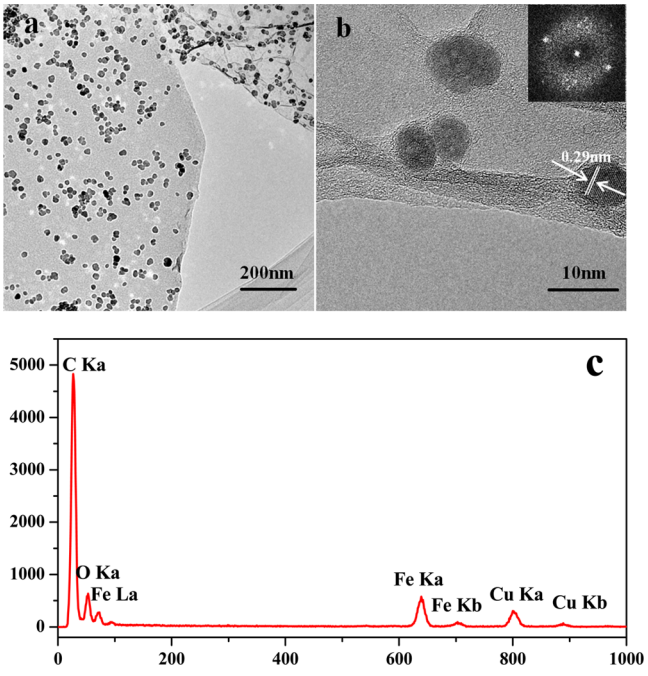

Figure 1. (a) Typical TEM image, (b) HRTEM image, and (c) the energy spectrum analysis of G-Fe_3O_4 nanocomposites. Inset in b is a typical electron diffraction pattern of G-Fe_3O_4.

Graphene, as a two-dimensional single sheet of carbon atoms arranged in a hexagonal network, has emerged as one of the most promising materials in water treatment because of its excellent mobility of charge carriers, large specific surface area, flexible structure, high transparency, and good electrical and thermal conduction.[15−17] In addition, graphene can be easily modified because of abundant oxygen functional groups on its surface, such as the combination of graphene and metal oxides, which can be applied in various fields such as catalysis,[18] lithium battery,[19] water treatment,[9,20,21] and so on. The graphene composites were used to remove metal heavy and organic dye; however, there is no report to cleaning pathogens bacteria in water with Fe_3O_4 modified graphene. On the other hand, graphene can prevent Fe_3O_4 agglomeration and enhance the removal efficiency because of its huge specific surface area and two-dimensional single-sheet structure.[22]

In the paper, Fe_3O_4/graphene (abbreviated as G-Fe_3O_4) has been successfully prepared through solvothermal method, which are applied to rapidly remove the microbial pathogens including both bacteriophage (bacteriophage ms2) and bacteria (six different species of Gram-positive and Gram-negative bacteria). Moreover, several process factors have been optimized to improve its removal efficiency, such as amount of G-Fe_3O_4 composite and incubation time. It can be found that bacteriophage and bacteria can be effectively removed from water using G-Fe_3O_4 composite. Furthermore, a detailed verification test of real water samples indicated that G-Fe_3O_4 composite still show high removal efficiency over pathogenic micoorganisms (both bacteria and bacteriophage).

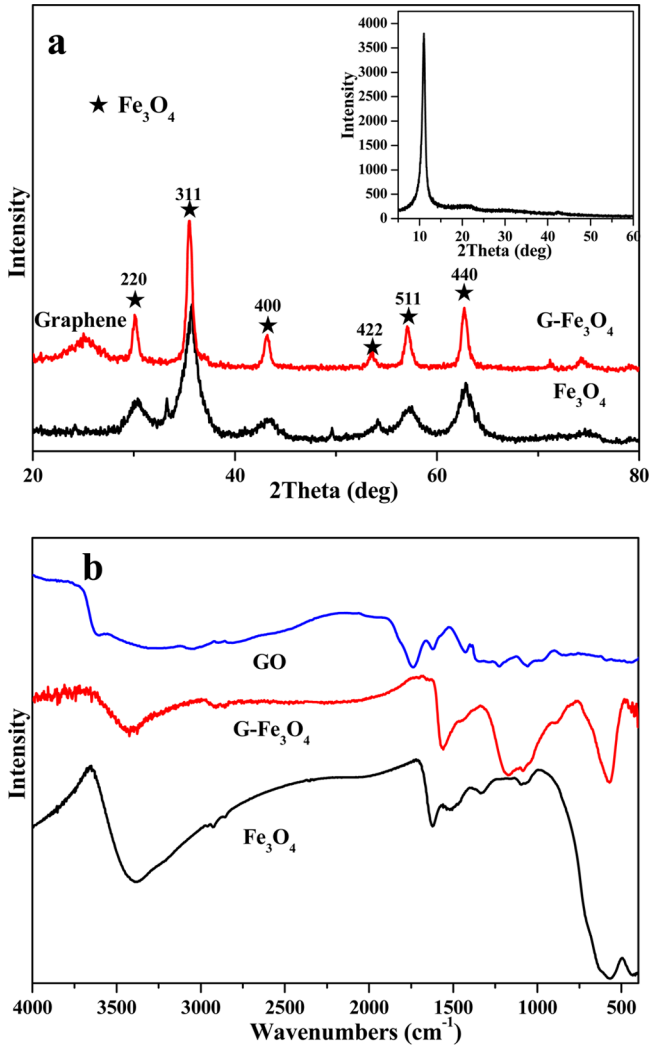

Figure 2. (a) XRD patterns of G-Fe_3O_4 and pure Fe_3O_4 (inset: XRD pattern of GO) and (b) FTIR spectra of graphene oxide (GO), G-Fe_3O_4, and pure Fe_3O_4.

DOI: 10.1021/am508682s
ACS Appl. Mater. Interfaces 2015, 7, 4290−4298

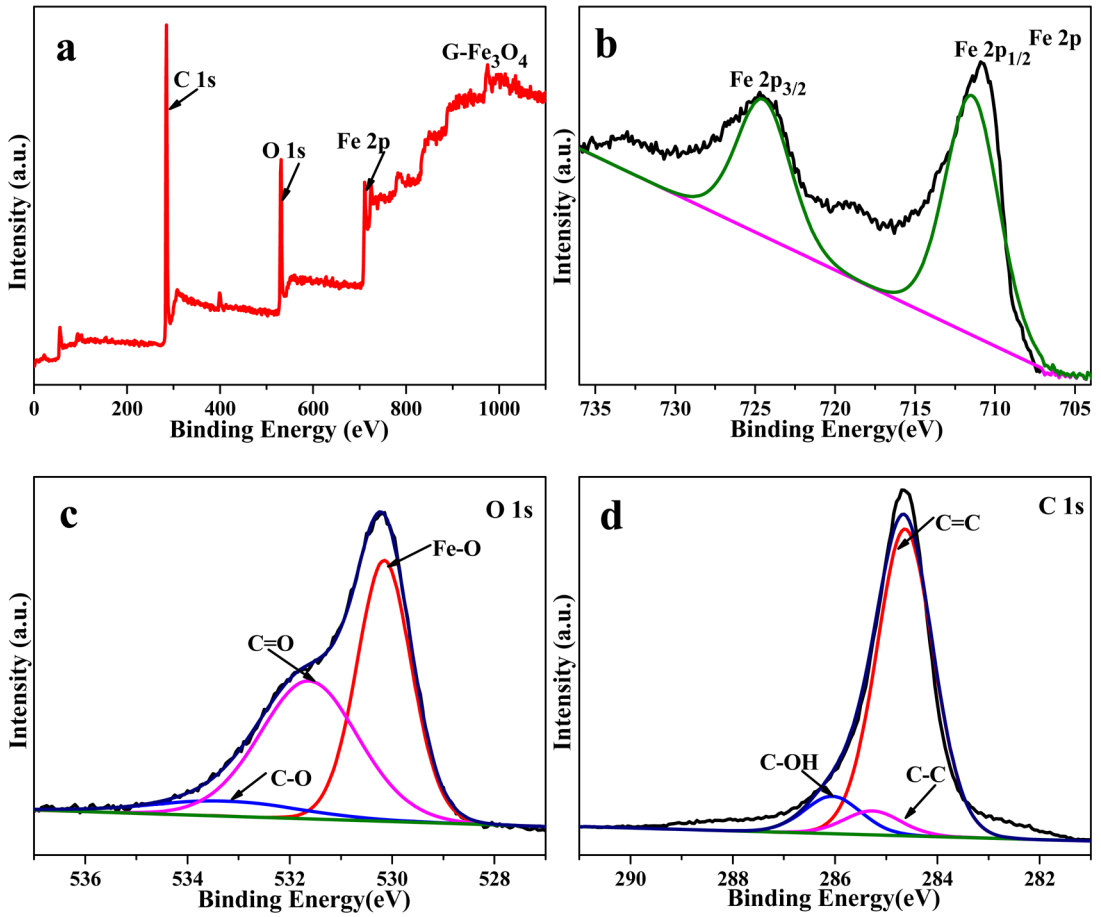

Figure 3. XPS spectrum of G-Fe_3O_4 composites: (a) full spectrum, (b) Fe 2p, (c) O 1s, (d) C 1s.

2. EXPERIMENTAL SECTION

2.1. Materials. All chemicals used here are analytical grade or higher. Ethylene glycol (EG), ammonium acetate (NH_4Ac), sulfuric acid (H_2SO_4), potassium permanganate ($KMnO_4$), 30% hydrogen peroxide (H_2O_2), sodium nitrate ($NaNO_3$) and graphite were purchased from Jiangtian Chemical Technology Co. Ltd. (Tianjin, China).

2.2. Synthesis of G-Fe_3O_4 Composite. Graphene oxide (GO) was prepared based on the earlier published paper.[23] As shown in Scheme 1, 0.225g of $Fe(acac)_3$ was added into the 45 mL of GO/EG (1 mg/mL). After ultrasonication for 30 min, 1.5 g of NH_4Ac was added into the above solution, and then the mixture was stirred for 30 min. The obtained mixture was then sealed in a Teflon-lined stainless steel autoclave and maintained at 200 °C for 24 h. After cooling to room temperature, the resulting black product was washed with deionized water several times and then dried at 60 °C.

As a comparison, pure Fe_3O_4 nanoparticles were also synthesized through same solvothermal method. In a typical synthesis of Fe_3O_4 nanoparticles, $Fe(acac)_3$ (0.03517g) was dissolved in a mixture of octylamine (4.0 mL) and octanol (12.0 mL). Then, the solution was transferred into a Teflon-lined autoclave. The autoclave was sealed and maintained at 240 °C for 2 h in an oven and naturally cooled to room temperature. The black precipitate was collected by centrifugation, followed by washing with ethanol and deionized water several times, and then dried at 60 °C.

2.3. Characteristic. The size and morphology of G-Fe_3O_4 were observed by transmission electron microscopy (TEM) using a JEOL model JEM-1200EX at 80 kV. The elemental analysis was carried out by using the energy-dispersive spectroscopy (EDS) facility of Hitachi JEOL model JEM-1200EX. The X-ray diffraction (XRD) patterns of samples were recorded via an X-ray diffractometer (Rigaku D/Max 2500PC) with a graphite monochromator and Cu$K\alpha$ radiation (γ= 0.15418 nm) at room temperature, with the voltage and electric current being fixed at 28 kV and 20 mA. FTIR spectra were recorded on a Nicolet 5DX-FTIR spectrometer using KBr pellet method in the range of 400−4000 cm^{-1}. X-ray photoelectron spectroscopy (XPS) spectra were collected on an ESCALAB250 multitechnique X-ray photoelectron spectrometer (UK) using a monochromatic Al Kα X-ray source ($h\nu$ = 1486.6 eV). All XPS spectra were recorded using an aperture slot of 300 μm × 700 μm, survey spectra were recorded with a pass energy of 160 eV, and high resolution spectra with a pass energy of 40 eV. N_2 adsorption−desorption data were obtained using a Quantachrom SI Micromeritics apparatus, and the isotherms were evaluated with the Barrett−Joyner−Halenda (BJH) theory to get the surface area, pore size and distribution. Zeta potentials were measured on a Malvern ZEN2600 Zetasizer Nano Z. The magnetic properties of the nanoparticles were studied using a vibrating sample magnetometer (LDJ 9600−1, USA) at room temperature by cycling the field from −2 to 2 kOe.

2.4. Removal Experiments of Microorganism. *2.4.1. Preparation of Bacterial Samples.* Stock cultures of *bacteriophage ms2*, *Staphylococcus aureus* (*S. aureus*), *Escherichia coli* (*E. coli*), *Salmonella*, *Enterococcus faecium* (*E. Faecium*), *Enterococcus faecalis* (*E. faecalis*), and *Shigella* were received from the Institute of Epidemiology and Microbiology, Academy of Preventive Medical Sciences, P.R. China. Then, the pure cultures of each bacterium were grown in nutrient broth at 37 °C for 24 h to yield a cell count of approximately 1 × 10^8 CFU/mL. At last, bacterial cells were collected by centrifugation (3000 rpm for 15 min) and resuspended in 20 mL of sterile 0.85% (wt/vol) saline solution. The sample concentration (0.05, 0.10, 0.15, 1.20, 0.25, 0.30, 0.35 mg/mL) appropriate for adsorption experiments was adjusted by gradient dilution using PBS (0.01 mM, pH7.0). For safety considerations, all of the samples were placed in an autoclave at 121 °C for 20 min before disposal and all glass-ware in contact with

DOI: 10.1021/am508682s
ACS Appl. Mater. Interfaces 2015, 7, 4290−4298

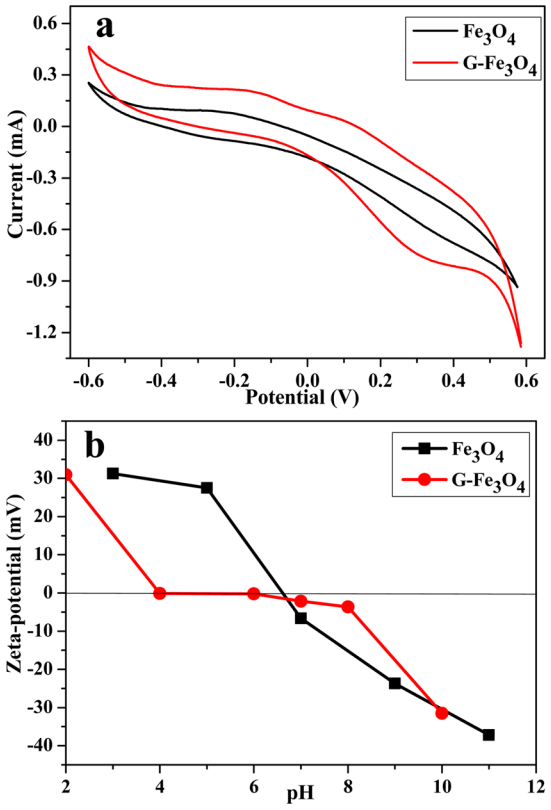

Figure 4. (a) Cyclic voltammetry curves using Fe_3O_4 and G-Fe_3O_4 as electrodes in 0.1 M sodium sulfate aqueous solution with a scanning rate of 0.05 V/s; (b) zeta potentials of Fe_3O_4 and G-Fe_3O_4.

sample was sterilized before and after usage. In the paper, the *E. coli* used as experiment modal was *E. coli* O157:H7.

2.4.2. Removal of Bacteria by G-Fe_3O_4. The bacterial concentration was diluted to a desired level (the amounts of bacteria was 1×10^2 CFU/mL), and 50 μL of a certain amount of G-Fe_3O_4 composites or Fe_3O_4 nanoparticles suspended in PBS (0.01 mM, pH 7.0) was then added into the bacterial solution (2 mL). The mixed solution was incubated by a rotary shaker at 250 rpm for 20 min so that nanomaterial can bind with the bacteria effectively, then the resulting nanocomposites-bacteria conjugates were magnetically confined for 10 min with an external magnet. The supernatant was then carefully pipetted out and determined by the conventional surface plate count method. As for the other bacterial pathogens, nutrient agar at a certain dilution (1.5%) was poured into the supernatant (1 mL) and shaken well. The plates were then incubated at 37 °C for 24 h. The number of colonies grown on the plates was enumerated and the initial bacterial solution was evaluated as control. The removal efficiencies of bacteria by G-Fe_3O_4 composites or Fe_3O_4 nanoparticles were calculated as follows

$$\text{removal efficiency}(\%) = \frac{\text{CFU}_0 - \text{CFU}_t}{\text{CFU}_0} \times 100\%$$

where CFU_0 and CFU_t are the initial and residual numbers of bacterial colonies in samples.

A series of experiments were conducted to investigate the effect of different factors for removal efficiency including sample concentrations (0.05, 0.10, 0.15, 1.20, 0.25, 0.30, 0.35 mg/mL), different bacteria concentrations (1×10^2, 1×10^4, 1×10^6 CFU/mL) and different time intervals.

The removal bacteria of GO is similar to G-Fe_3O_4 nanoparticles. The only difference was that GO-bacteria conjugates was not separated because of the difficult separation of GO.

2.4.3. Fluorescent-Based Cell Live/Dead Test. The bacteria death analysis was investigated by fluorescent-based cell live/dead test.

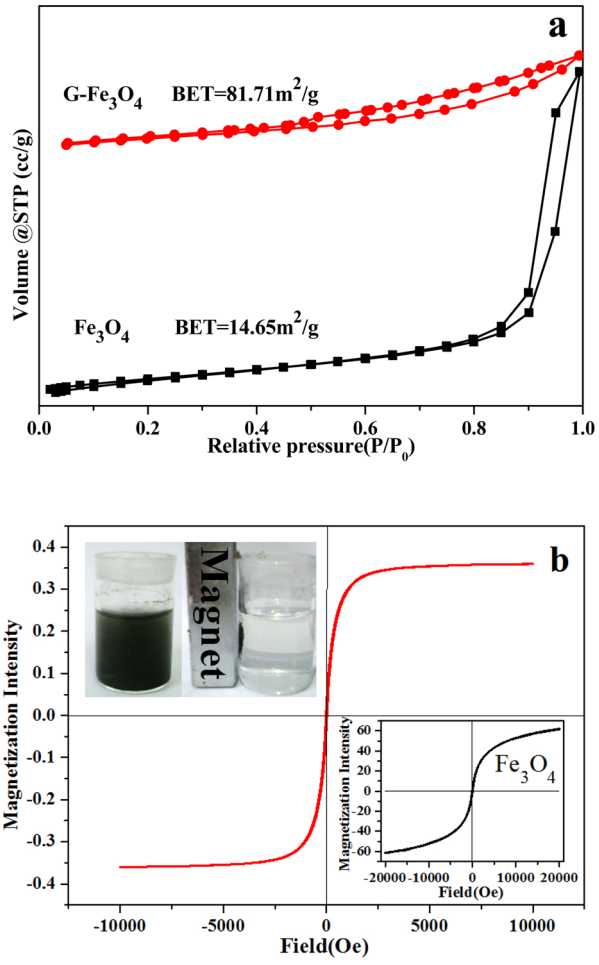

Figure 5. (a) N_2 adsorption−desorption isotherms and (b) room-temperature magnetization curves of G-Fe_3O_4 and Fe_3O_4. As shown in the inset in b, the G-Fe_3O_4 can be separated from water with an external magnet.

The mixture of log phase cells (1×10^8 CFU) and 50 μg/mL of sample were incubated by a rotary shaker at 250 rpm for 20 min. Then nanomaterials were separated magnetically and the cells were collected by centrifugation and washed with 0.85% (wt/vol) saline solution three times. Then the cells were stained with PI and SYTO9 (LIVE/DEAD Baclight Bacterial Viability kit) according to the instruction of the kit, then imaged using a laser scanning fluorescence microscopy (Olympus, FV1000). SYTO9 was a cell-permeable green-fluorescent stain labeled both live and dead bacteria, whereas PI was a cell-impermeable red-fluorescent stain that only labeled dead bcateria.

3. RESULTS AND DISCUSSION

3.1. Characteristic of G-Fe_3O_4. The typical TEM images of G-Fe_3O_4 are shown in Figure 1. From Figure 1a, it is clearly observed that the about 10 nm Fe_3O_4 nanoparticles are combined with graphene nanosheets with narrow particle size and uniform dispersion. Thus, the presence of graphene helps prevent pure Fe_3O_4 from agglomeration, which is conducive to the removal of pathogens. In addition, it is obvious that the graphene show folding nature, which is in agreement with the earlier study.[24,25] As illustrated in the typical HRTEM image of G-Fe_3O_4 (Figure 1b), lattice fringes of Fe_3O_4 (d = 0.29 nm) can be found clearly, demonstrating that Fe_3O_4 sample is highly crystalline. Furthermore, the electron diffraction patterns of G-Fe_3O_4 (inset of Figure 1b) can be indexed to the highly crystalline reflections of cubic inverse spinel Fe_3O_4 structure,

DOI: 10.1021/am508682s
ACS Appl. Mater. Interfaces 2015, 7, 4290−4298

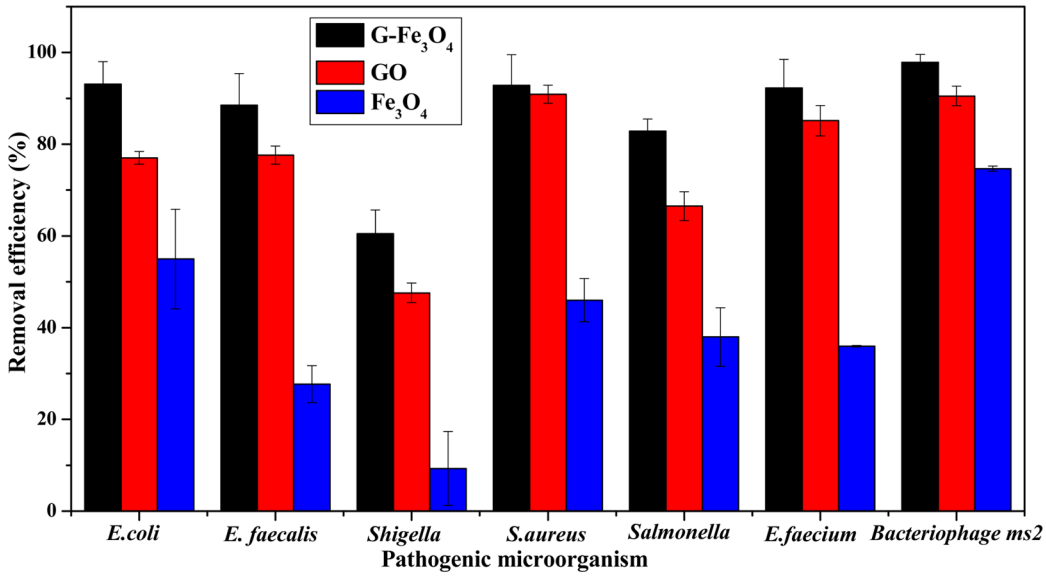

Figure 6. Nonspecific removal of *bacteriophage ms2; bacteria: E. coli, E. faecalis, Shigella, S. aureus, Salmonella, E. faecium.*

which is in accordance with the below result of XRD. In addition, energy-dispersive spectroscopy (EDS) was also conducted to analyze the chemical composition of G-Fe_3O_4, which obviously proves that G-Fe_3O_4 nanocomposites are composed with C, Fe, and O elements. Furthermore, the existence of Cu peak in EDS spectrum come from the copper mesh used in TEM tests. However, the presence of C originates not only from G-Fe_3O_4 but also from the copper mesh.

In the XRD patterns (Figure 2a), pentagram represents characteristic peaks of spinel Fe_3O_4. From the XRD patterns (Figure 2a), it is obvious that the diffraction peaks of pure Fe_3O_4 can be indexed to (220), (311), (400), (422), (511), and (440) planes appearing at 2θ = 30.1, 35.5, 43.1, 53.4, 57.0, and 62.6°, which is in accordance with the database of JCPDS (PDF#89−0691).[21,23] Compared with pure Fe_3O_4, the XRD pattern of G-Fe_3O_4 show an extra largely shoulder centered at 25°, which can be attributed to the presence of graphene and consist with the published report, clearly confirmed the good combination between graphene and Fe_3O_4.[26,27] By the way, on the basis of the Scherrer equation, the crystallite dimension ranges from 15 to 25 nm. Thus, the small size is beneficial for the following removal of microorganism.

The FTIR spectra of GO, G-Fe_3O_4, and Fe_3O_4 are as shown in Figure 2b. All samples show broad bands at 3378 and 1558 cm^{-1}, which can be assigned to the −OH group and the H−O−H stretching and bending vibrations of the adsorbed water molecules.[28] For G-Fe_3O_4 and Fe_3O_4, the characteristic peaks of 582 and 453 cm^{-1} is attributed to the Fe−O vibrations, which confirmed the presence of Fe_3O_4.[27] It is easy to observe that the peaks of GO ranging from 750 to 1750 cm^{-1} have many oxygen-containing functional moieties, including the peak of the C−O stretching vibration of epoxide, tertiary C−OH groups stretching and C═O stretching of carbonyl and carboxyl groups.[23] However, for G-Fe_3O_4 composite, these peaks of oxygen-containing functional moieties decreased and even disappeared, indicating that the GO was reduce to graphene. And the peaks at the 1184 and 1081 cm^{-1} also confirmed the existence of some oxygen-containing functional moieties on the surface G-Fe_3O_4 composite after GO was reduced.

To further understand the composition of G-Fe_3O_4 and the valence of different element, the XPS spectrum of G-Fe_3O_4 are as shown in Figure 3. In Figure 3a, the three different major peaks can be assigned to Fe 2p, O 1s, and C 1s, respectively, indicating that the G-Fe_3O_4 contains Fe, O and C element, which is consistent with the result of element analysis. As shown in Figure 3b, it is obvious that the two peaks at 711.4 and 724.5 eV are assigned to the Fe $2p_{1/2}$ and Fe $2p_{3/2}$ of Fe_3O_4.[29] From Figure 3c, after a peak-fitting deconvolution, the O 1s of G-Fe_3O_4 can be separated into three peaks with the anionic oxygen in Fe−O (at 530.1 eV), the carbonyl oxygen in C═O (at 531.6 eV), and the oxygen in C−O at (at 533.2 eV), which show that some surface oxygen groups still exist in reduced graphene surface.[26,30] The C 1s XPS spectrum of G-Fe_3O_4 can also be decomposable into three spectral components, C═C (at 284.6 eV), C−C (at 285.3 eV), and C−OH (at 286.0 eV), which also confirmed that surface oxygen groups on graphene oxide will not completely disappear after graphene oxide was reduced.[31]

Cyclic voltammetry curves were performed by through of a three-electrode system with modified aluminum plate (prepared by dipcoating and dry it in air at room temperature) as the working electrode, a platinum plate as the counter electrode and Ag/AgCl electrode as the reference electrode.[32] Then, the electrochemical performance of Fe_3O_4 and G-Fe_3O_4 was evaluated by cyclic voltammetry. As shown in Figure 4a, current with different contents at Fe_3O_4 and G-Fe_3O_4 modified aluminum electrodes came into being. It is obvious that the CV loop of G-Fe_3O_4 was broader than pure Fe_3O_4, demonstrating that the conductivity of pure Fe_3O_4 became higher after adding graphene because of its high electrical conductivity.[33,34] The results also confirmed the good combination with graphene and Fe_3O_4.

The charge state of pure Fe_3O_4 nanoparticles will be different from G-Fe_3O_4 composite, the zeta potentials analysis was further carried out, as shown in Figure 4b. The isoelectric point (IEP) of Fe_3O_4 nanoparticles was 6.61 (pH value), whereas the isoelectric point (IEP) of G-Fe_3O_4 composite became 4.00 (pH value) after doping graphene, which may be due to the surface oxygen groups on graphene.[23−25,28] The higher isoelectric point (IEP) is helpful for increasing the removal efficiency of pathogens. However, the removal efficiency of pathogens for G-Fe_3O_4 composite is higher than pure Fe_3O_4 nanoparticles, which may

DOI: 10.1021/am508682s
ACS Appl. Mater. Interfaces 2015, 7, 4290−4298

be due to the others factors such as huge specific surface area and good dispersion.

To investigate the porous structure and surface area of G-Fe_3O_4 and Fe_3O_4, we conducted the N_2 adsorption−desorption isotherms, as shown in Figure 5a, which also exactly explain the extremely high removal efficiency of G-Fe_3O_4 compared with Fe_3O_4. The N_2 adsorption−desorption curve of Fe_3O_4 can be classified to typical Type II without hysteresis loop, which is the characteristic of nonporous materials.[22,27] However, the curve of G-Fe_3O_4 is close to type IV with a weak hysteresis loop in the 0.4−1.0 range of relative pressure, which indicated the presence of porous structure of G-Fe_3O_4 composite.[23] In addition, compared with the pure Fe_3O_4, the specific surface area of G-Fe_3O_4 significantly increased from 14.65m^2/g to 81.71m^2/g, which indicates that more functional active sites exited in the surface of G-Fe_3O_4. Thus, this confirmed that the existence of graphene not only have prevented the Fe_3O_4 from agglomeration, but also have increased the specific surface area, which is accordant with TEM results. The more active sites of G-Fe_3O_4 and higher specific surface area will help G-Fe_3O_4 exhibit higher removal efficiency for pathogens, which can be confirmed by the following experiment results.

To evaluate the magnetic separation capacity of G-Fe_3O_4, we conducted the magnetic hysteresis loops of G-Fe_3O_4 and pure Fe_3O_4 at room temperature, as shown in Figure 5b. The magnetic saturation (M_s) value of the pure Fe_3O_4 nanoparticles was 61.76 emu/g, whereas the magnetic saturation (M_s) value of the G-Fe_3O_4 composite gradually decreased to 0.359 emu/g, which is due to the sharply reduced relative content of Fe_3O_4. As shown in the upper left image of Figure 5b, G-Fe_3O_4 composite can be rapidly separated from the black and stable suspension solution with a help of an external magnet, which is important for recycling and reusing these absorbents. Thus, the magnetic saturation (M_s) value of the G-Fe_3O_4 composite was lower than pure Fe_3O_4 nanoparticles, but the magnetic separation capacity was still strong enough to separate them.

3.2. Nonspecific Removal of Pathogenic Bacteria and Bacteriophage. It is reported that the infectious dose of *E. coli O157:H7* is possibly less than 100 colony-forming units (CFU). The waters were regarded as being polluted once the concentration of *E. coli O157:H7* higher than 100 CFU/mL. Thus, pathogenic bacteria concentration with 10−100 CFU/mL was chosen as the appreciate concentration to conduct the removal experiment.[8] The removal experiments of pathogenic bacteria were all done for G-Fe_3O_4, GO, or Fe_3O_4 at a cell concentration of 1×10^2 CFU/mL under the condition (pH 7, the concentration of composites in bacterial solution is 0.25 mg/mL). As shown in Figure 6, it is clearly seen that G-Fe_3O_4 composite can quickly clean at least 6 different typical species of Gram-positive (*S. aureus*, *E. faecalis*, and *E. faecium*) and Gram-negative bacteria (*E. coli*, *Shigella*, and *Salmonella*) with a higher removal efficiency of 92.79, 88.52, 92.26, 93.09, 60.49, and 82.85%, respectively. At the same time, it can be seen that the removal efficiency for bacteria with GO is also higher, which is due to its excellent antibacterial properties. However, it is slightly lower than G-Fe_3O_4 composites and is very difficult to be separated from water. Therefore, G-Fe_3O_4 composites were prepared and studied carefully here. The antibacterial property of GO has been extensively investigated in the earlier reported.[35,36] However, the removal efficiency of pure Fe_3O_4 composites for these 6 different bacteria were all lower than G-Fe_3O_4 composites, which may be attributed to the huge specific surface area of G-Fe_3O_4, excellent monodisperse of Fe_3O_4 on the surface of graphene, and the antibacterial effect of graphene.[37,38] In addition, the removal efficiency of G- Fe_3O_4 for *bacteriophage ms2* can achieve 97.84%. All of the above results directly explain the benefits of graphene on the water treatment.

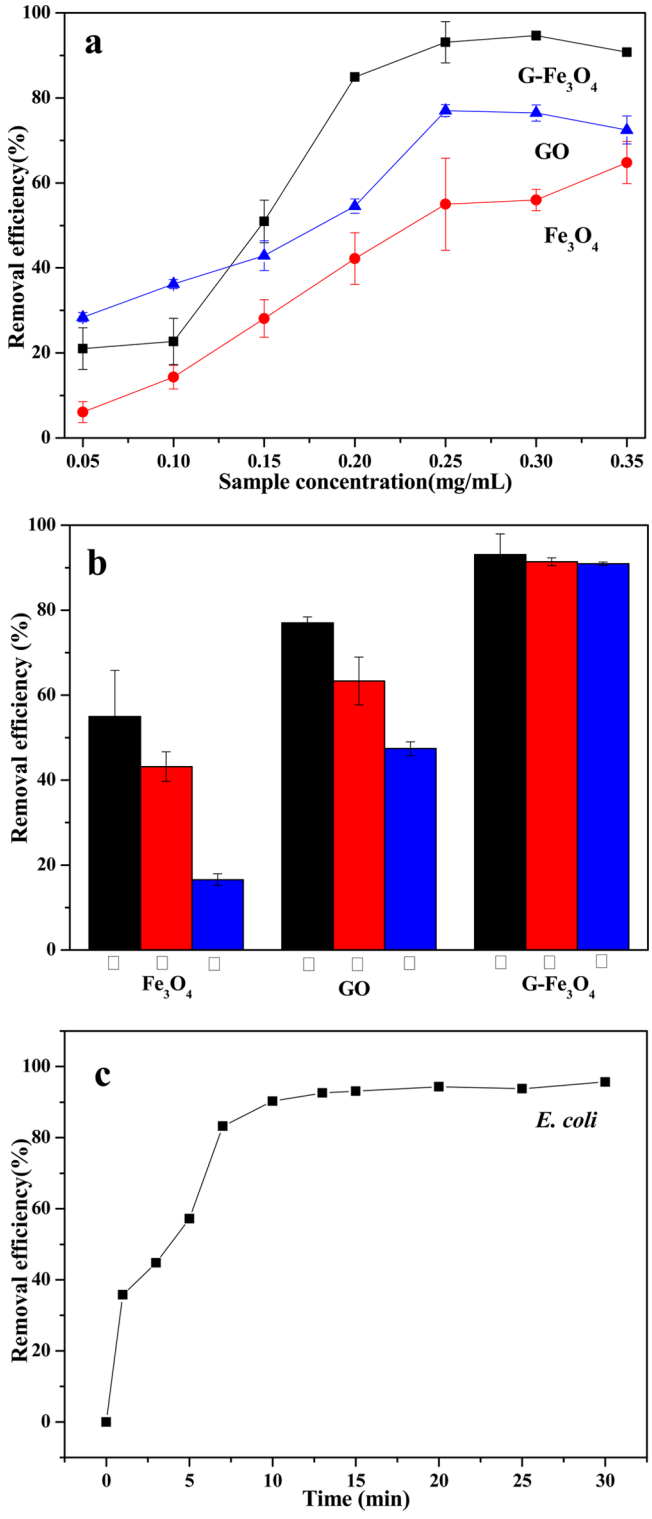

Figure 7. Influencing factors on (a) removal rate of the concentration of G-Fe_3O_4, GO, or Fe_3O_4 and (c) incubation time. (b) Removal efficiency of G-Fe_3O_4, GO and Fe_3O_4 in different concentration of bacteria (I, 1×10^2 CFU/mL; II, 1×10^4 CFU/mL; III, 1×10^6 CFU/mL).

DOI: 10.1021/am508682s
ACS Appl. Mater. Interfaces 2015, 7, 4290−4298

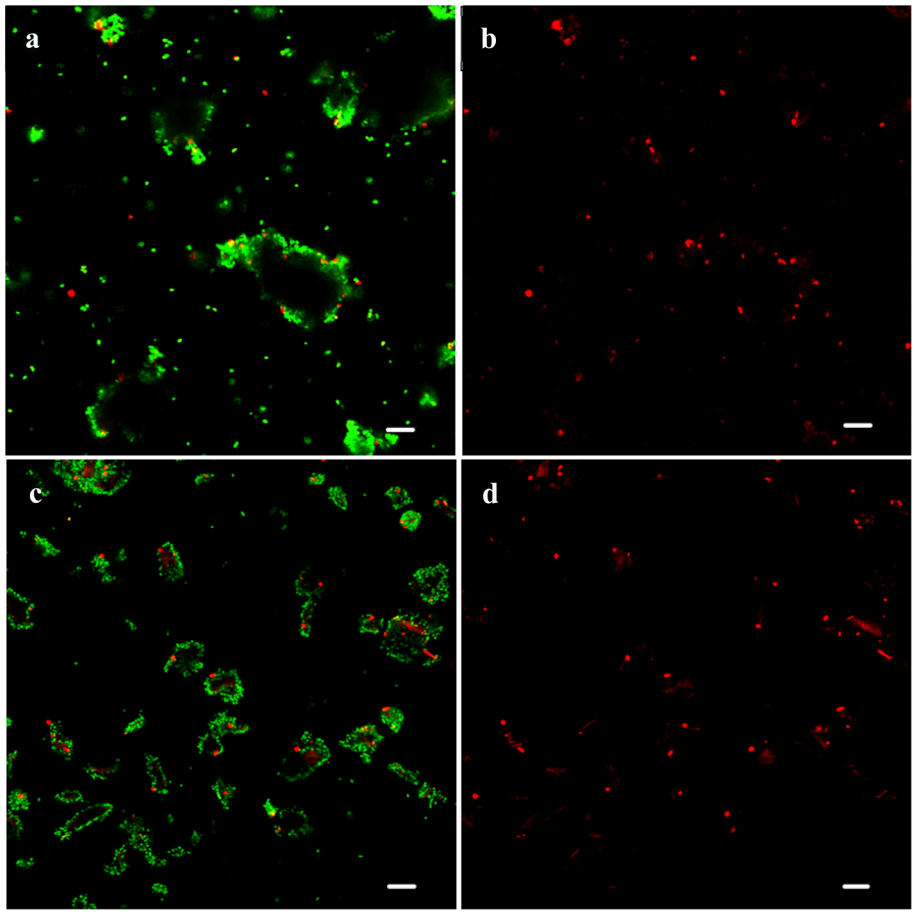

Figure 8. Confocal fluorescent images of live and dead bacterial cells after incubation with 2.5 mg/mL of (a, b) G-Fe_3O_4 and (c, d) GO for 20 min, and subsequently stained briefly (20 min) with SYTO9 (green) and PI (red). Scale bar = 10 μm.

3.3. Influence Factors. A series of experiments were performed to discover the optimal conditions to remove microbial pathogenic pathogens using *E. coli O157:H7* as model microorganism, by changing absorbent concentration, bacteria concentration and the incubation time.

The effect of the amount of G-Fe_3O_4 composite on the removal efficiency of *E. coli* O157:H7 was examined by varying amounts of G-Fe_3O_4 composite to bacterial suspensions (0.01 mM PBS, pH 7.0) with a bacteria concentration of 10^2 CFU/mL. The G-Fe_3O_4 composite were separated from bacteria solution with an outside magnet after 15 min. From Figure 7a, the fact that the removal efficiency of G-Fe_3O_4 composite, GO, or Fe_3O_4 composites became higher with the increasing of the amount of G-Fe_3O_4 composite, GO or Fe_3O_4 composites can be observed clearly, and the removal efficiency reached highest at the concentration of G-Fe_3O_4 composite, GO or Fe_3O_4 composites with 0.25 mg/mL, which is obviously due to the increased active surface sites.[39,40] However, the removal efficiency of G-Fe_3O_4 composite for *E. coli* was much higher than Fe_3O_4 composites at each concentration level, which is due to the huge specific surface area of G-Fe_3O_4 composite and good monodisperse of Fe_3O_4 on the surface of graphene. As we all know, GO had high removal efficiency for bacteria because of its strong antibacterial properties; however, it is very difficult to separate used GO from water. Therefore, G-Fe_3O_4 composite will have more application prospects because of its higher removal efficiency for bacteria and easy separation from water with an outer magnet.

To evaluate the removal efficiency of G-Fe_3O_4, GO, and Fe_3O_4 on high concentration of bacteria, the mixed suspension (PBS 0.01 mM, pH 7.0) of different concentration (1×10^2 CFU/mL, 1×10^4 CFU/mL, and 1×10^6 CFU/mL) *E. coli* and 0.25 mg/mL G-Fe_3O_4 composite were shaken on a rotary shaker at 250 rpm. As shown in Figure 7b, all nanomaterials show higher removal efficiency on 1×10^2 CFU/mL bacteria concentration than 10^4 and 10^6 CFU/mL bacteria concentration. However, for G-Fe_3O_4 composite, it is obvious that all of the removal efficiency on the three different bacteria concentration (1×10^2 CFU/mL, 1×10^4 CFU/mL, and 1×10^6 CFU/mL) were more than 90%, and the 93% removal efficiency for 10^2 CFU/mL was slightly higher than 91% removal efficiency for 10^4 CFU/mL and 90% removal efficiency for 1×10^6 CFU/mL, respectively. Therefore, G-Fe_3O_4 composite showed high removal efficiency on either high concentration bacteria or low concentration bacteria.

To evaluate the effect of incubation time on removal efficiency, we shook the mixed suspension (PBS 0.01 mM, pH 7.0) of *E. coli* and G-Fe_3O_4 composite with a concentration of 0.25 mg/mL on a rotary shaker at 250 rpm for different time interval. As shown in Figure 7b, it is observed that the concentration of *E. coli* in supernatant solution decreases gradually with the increasing incubation time and the removal efficiency reached more than 90% after 10 min, which is assigned to the sufficient contact time of G-Fe_3O_4 and *E. coli* solution.

3.4. Removal Tests of Real Water Samples. In practice, the real water samples are different from the simulated water. Thus, we further investigate the removal capability of the

DOI: 10.1021/am508682s
ACS Appl. Mater. Interfaces 2015, 7, 4290−4298

G-Fe_3O_4 composites toward pathogenic microorganisms (both bacteria and bacteriophage) in real water samples through a microbial plate count method. The result of removal efficiency for G-Fe_3O_4 composite was obtained through averaged values after several tests. The real samples were collected from local rivers (Dayun River, Tianjin, China). First, the G- Fe_3O_4 nanoparticles were allowed to contact with target water samples for 15 min. Then, the resulting conjugates were separated, diluted, and cultured on a LB plate for 24 h at 37 °C. As a result, we found that G-Fe_3O_4 composite have extremely high capture capability for both bacteria and bacteriophage, the CFUs in a 1 mL water sample before and after treatment with G-Fe_3O_4 composite were 1745 and 89, respectively. Therefore, the removal efficiency for bacteria can achieve 94.8% in the studied water samples. The bacteriophage plaque in a 1 mL water sample before and after treatment with G-Fe_3O_4 composite were 2.7×10^9 and 1×10^8. Therefore, the removal efficiency for bacteriophage can reach 96.3%.

3.5. Removal Mechanism. To the best of our knowledge, it is reported that GO and graphene showed strong antibacterial properties.[41,42] Therefore, to investigate the removal mechanism of G-Fe_3O_4 composites, Fluorescent-based cell live/dead test of live and dead bacterial cells were conducted, as shown in Figure 8. The SYTO 9 enters through the bacteria membrane and makes them green color for both living and dead bacteria, whereas the propodium iodide (PI) gives red color for dead bacteria because of the damaged cell wall membrane caused by photothermal lysis. In Figure 8, it can be observed that many bacteria were stained by PI, indicating damaged cell walls and cell membranes or mass cell death upon GO or G-Fe_3O_4 composites exposure. In Figure 8a, c, it can be clearly observed that many bacteria adhered to the surface of G-Fe_3O_4 composites or GO. In addition, there are a lot of dead bacteria on the surface of G-Fe_3O_4 composites or GO, which directly confirmed the antibacterial properties of G-Fe_3O_4 composites or GO. However, the amount of dead bacteria on the GO surface is more than G-Fe_3O_4 composites due to its relative lower content of graphene for G-Fe_3O_4 composites compared with GO, which indicated the antibacterial properties of graphene in the G-Fe_3O_4 composites. In addition, it can be observed that the amount of live bacteria is more than the amount of dead bacteria based on confocal fluorescent images. Therefore, for G-Fe_3O_4 composites, the removal mechanism is mainly due to the adsorbability; the second is its antibacterial properties of graphene.

4. CONCLUSION

In conclusion, Fe_3O_4/graphene (abbreviated as G-Fe_3O_4) nanoparticles was synthesized successfully by solvothermal method to effectively remove both bacteriophage and bacteria. The removal efficiency of *E. coli* for G-Fe_3O_4 composite can achieve 93.09%, whereas it is only 54.97% with Fe_3O_4 nanoparticles. In addition, the G-Fe_3O_4 composite show high removal efficiency for a wide range of pathogens including not only *bacteriophage ms2*, but also various bacteria such as *S. aureus*, *E. coli*, *Salmonella*, *E. Faecium*, *E. faecalis*, and *Shigella*. Moreover, a detailed verification test of real water samples was conducted and the removal efficiency of bacteria in real water for G-Fe_3O_4 composite can also reach 94.8%. The removal mechanism of G-Fe_3O_4 was also investigated.

AUTHOR INFORMATION

Corresponding Authors

*E-mail: sihuizhan@nankai.edu.cn. Tel/Fax: +86-22-23502756.
*E-mail: szq922990@126.com

Notes

The authors declare no competing financial interest.

ACKNOWLEDGMENTS

The authors gratefully acknowledge the financial support provided by the National Natural Science Foundation of China (21377061, 21003094), the Asia Research Center in Nankai University (AS1326), the Natural Science Foundation of Tianjin (12JCQNJC05800), and the Key Technologies R&D Program of Tianjin (13ZCZDSF00300) and the assistance provided by Dr. Raymond Seekell (University of Notre Dame) in the manuscript preparation and discussion.

REFERENCES

(1) Liu, C.; Xie, X.; Zhao, W.; Liu, N.; Maraccini, P. A.; Sassoubre, L. M.; Boehm, A. B.; Cui, Y. Conducting Nanosponge Electroporation for Affordable and High-Efficiency Disinfection of Bacteria and Viruses in Water. *Nano Lett.* **2013**, *13*, 4288−4293.
(2) Ma, X.; Zhou, W.; Fu, Z.; Cheng, Y.; Min, M.; Liu, Y.; Zhang, Y.; Chen, P.; Ruan, R. Effect of Wastewater-Borne Bacteria on Algal Growth and Nutrients Removal in Wastewater-Based Algae Cultivation System. *Bioresour. Technol.* **2014**, *167*, 8−13.
(3) Deng, D.; Zhang, N.; Mustapha, A.; Xu, D.; Wuliji, T.; Farley, M.; Yang, J.; Hua, B.; Liu, F.; Zheng, G. Differentiating Enteric Escherichia coli from Environmental Bacteria Through the Putative Glucosyltransferase Gene (ycjM). *Water Res.* **2014**, *61*, 224−231.
(4) Chung, H. J.; Reiner, T.; Budin, G.; Min, C.; Liong, M.; Issadore, D.; Lee, H.; Weissleder, R. Ubiquitous Detection of Gram-Positive Bacteria with Bioorthogonal Magnetofluorescent Nanoparticles. *ACS Nano* **2011**, *5*, 8834−8841.
(5) Jin, Y.; Liu, F.; Shan, C.; Tong, M.; Hou, Y. Efficient bacterial capture with Amino Acid Modified Magnetic Nanoparticles. *Water Res.* **2014**, *50*, 124−134.
(6) Yuan, Q.; Li, N.; Chi, Y.; Geng, W.; Yan, W.; Zhao, Y.; Li, X.; Dong, B. Effect of Large Pore Size of Multifunctional Mesoporous Microsphere on Removal of Heavy Metal Ions. *J. Hazard. Mater.* **2013**, *254*−*255*, 157−165.
(7) Pavagadhi, S.; Tang, A. L.; Sathishkumar, M.; Loh, K. P.; Balasubramanian, R. Removal of Microcystin-LR and Microcystin-RR by Graphene Oxide: Adsorption and Kinetic Experiments. *Water Res.* **2013**, *47*, 4621−4629.
(8) Pal, S.; Joardar, J.; Song, J. Removal of E. coli from Water Using Surface-Modified Activated Carbon Filter Media and Its Performance over an Extended Use. *Environ. Sci. Technol.* **2006**, *40*, 6091−6097.
(9) Vadahanambi, S.; Lee, S. H.; Kim, W. J.; Oh, I. K. Arsenic Removal from Contaminated Water Using Three-Dimensional Graphene-Carbon Nanotube-Iron Oxide Nanostructures. *Environ. Sci. Technol.* **2013**, *47*, 10510−10517.
(10) Zhao, H.; Li, G.; Liu, X.; Zhang, H.; An, T.; Zhang, S.; Carroll, A. R. In Situ Photoelectrocatalytic Generation of Bactericide for Instant Inactivation and Rapid Decomposition of Gram-Negative Bacteria. *J. Catal.* **2011**, *277*, 88−94.
(11) Zhang, H.; Fan, X.; Quan, X.; Chen, S.; Yu, H. Graphene sheets grafted Ag@AgCl Hybrid with Enhanced Plasmonic Photocatalytic Activity Under Visible Light. *Environ. Sci. Technol.* **2011**, *45*, 5731−5736.
(12) Heilshorn, S. C.; Schoen, A. P.; Schoen, D. T.; Huggins, K. N. L.; Arunagirinathan, M. A. Template Engineering Through Epitope Recognition: A Modular, Biomimetic Strategy for Inorganic Nanomaterial Synthesis. *J. Am. Chem. Soc.* **2011**, *133*, 18202−18207.
(13) He, H.; Gao, C. Supraparamagnetic, conductive, and Processable Multifunctional Graphene Nanosheets Coated with High-Density Fe_3O_4 Nanoparticles. *ACS Appl. Mater. Interfaces* **2010**, *2*, 3201−3210.
(14) Robatjazi, S. M.; Shojaosadati, S. A.; Khalilzadeh, R.; Farahani, E. V.; Balochi, N. Immobilization of Magnetic Modified Flavobacterium ATCC 27551 Using Magnetic Field and Evaluation of the

DOI: 10.1021/am508682s
ACS Appl. Mater. Interfaces 2015, 7, 4290−4298

Enzyme Stability of Immobilized Bacteria. *Bioresour. Technol.* **2012**, *104*, 6−11.
(15) Geim, A. K. Graphene: Status and Prospects. *Science* **2009**, *324*, 1530−1534.
(16) Wu, H. C.; Chang, H. X. Graphene-Based Nanocomposites: Preparation, Functionalization, and Energy and Environmental Applications. *Energy Environ. Sci.* **2013**, *6*, 3483−3507.
(17) Hu, X.; Zhou, Q. Health and Ecosystem Risks of Graphene. *Chem. Rev.* **2013**, *113*, 3815−3835.
(18) Morales-Torres, S.; Pastrana-Martinez, L. M.; Figueiredo, J. L.; Faria, J. L.; Silva, A. M. Design of Graphene-Based TiO_2 Photocatalysts–A Review. *Environ. Sci. Pollut. Res. Int.* **2012**, *19*, 3676−3687.
(19) Sun, X. L.; Yang, J. L.; Wang, J. J.; Tang, Y. J.; Wang, D. N.; Li, X. F.; Hu, Y. H.; Li, R. Y.; Liang, G. X.; Sham, T. K. $LiFePO_4$-graphene as a Superior Cathode Material for Rechargeable Lithium Batteries: Impact of Stacked Graphene and Unfolded Graphene. *Energy Environ. Sci.* **2013**, *6*, 1521−1528.
(20) Chowdhury, I.; Duch, M. C.; Mansukhani, N. D.; Hersam, M. C.; Bouchard, D. Colloidal Properties and Stability of Graphene Oxide Nanomaterials in the Aquatic Environment. *Environ. Sci. Technol.* **2013**, *47*, 6288−6296.
(21) Li, J.; Zhang, S.; Chen, C.; Zhao, G.; Yang, X.; Li, J.; Wang, X. Removal of Cu(II) and Fulvic Acid by Graphene Oxide Nanosheets Decorated with Fe_3O_4 Nanoparticles. *ACS Appl. Mater. Interfaces* **2012**, *4*, 4991−5000.
(22) Cheng, H. M.; Zhou, G. M.; Wang, D. W.; Li, F.; Zhang, L. L.; Li, N.; Wu, Z. S.; Wen, L.; Lu, G. Q. Graphene-Wrapped Fe_3O_4 Anode Material with Improved Reversible Capacity and Cyclic Stability for Lithium Ion Batteries. *Chem. Mater.* **2010**, *22*, 5306−5313.
(23) Zhang, H.; Li, X.; Huang, X.; Liu, D.; Wang, X.; Song, S.; Zhou, L. Synthesis of 3D Hierarchical Fe_3O_4/Graphene Composites with High Lithium Storage Capacity and for Controlled Drug Delivery. *J. Phys. Chem. C* **2011**, *115*, 21567−21573.
(24) Bhowmik, K.; Mukherjee, A.; Mishra, M. K.; De, G. Stable Ni Nanoparticle-Reduced Graphene Oxide Composites for the Reduction of Highly Toxic Aqueous Cr(VI) at Room Temperature. *Langmuir* **2014**, *30*, 3209−3216.
(25) Zhu, J.; Wei, S.; Gu, H.; Rapole, S. B.; Wang, Q.; Luo, Z.; Haldolaarachchige, N.; Young, D. P.; Guo, Z. One-pot synthesis of Magnetic Graphene Nanocomposites Decorated with core@double-shell nanoparticles for Fast Chromium Removal. *Environ. Sci. Technol.* **2012**, *46*, 977−985.
(26) Cheng, J.; Zhang, M.; Wu, G.; Wang, X.; Zhou, J.; Cen, K. Photoelectrocatalytic Reduction of CO_2 into Chemicals Using Pt-Modified Reduced Graphene Oxide Combined with Pt-modified TiO_2 Nanotubes. *Environ. Sci. Technol.* **2014**, *48*, 7076−7084.
(27) Hu, C. W.; Su, J.; Cao, M. H.; Ren, L. Fe_3O_4 Graphene Nanocomposites with Improved Lithium Storage and Magnetism Properties. *J. Phys. Chem. C* **2011**, *115*, 14469−14477.
(28) Zhan, S.; Yang, Y.; Shen, Z.; Shan, J.; Li, Y.; Yang, S.; Zhu, D. Efficient Removal of Pathogenic Bacteria and Viruses by Multifunctional Amine-Modified Magnetic Nanoparticles. *J. Hazard. Mater.* **2014**, *274*, 115−123.
(29) Xue, J. M.; Chen, Y.; Song, B.; Tang, X.; Lu, L. One-step Synthesis of Hollow Porous Fe_3O_4 Beads-Reduced Graphene Oxide Composites with Superior Battery Performance. *J. Mater. Chem.* **2012**, *22*, 17656−17662.
(30) Wang, X. P.; Geng, Z. G.; Lin, Y.; Yu, X. X.; Shen, Q. H.; Ma, L.; Li, Z. Y.; Pan, N. Highly Efficient Dye Adsorption and Removal: A Functional Hybrid Of Reduced Graphene Oxide-Fe_3O_4 Nanoparticles as an Easily Regenerative Adsorbent. *J. Mater. Chem.* **2012**, *22*, 3527−3535.
(31) Xi, P.; Huo, X.; Liu, J.; Wang, B.; Zhang, H.; Yang, Z. Y.; She, X. A One-Step Method to Produce Graphene-Fe_3O_4 Composites and Their Excellent Catalytic Activities for Three-Component Coupling of Aldehyde, Alkyne and Amine. *J. Mater. Chem. A* **2013**, *1*, 651−656.
(32) Lu, B. P.; Zhang, Z.; Hao, J. H.; Tang, J. L. Facile Synthesis of Au@Fe_3O_4-Graphene and Pt@Fe_3O_4-Graphene Ternary Hybrid Nanomaterials and Their Catalytic Properties. *RSC Adv.* **2014**, *4*, 21909−21917.
(33) Sun, J.; Liu, M. In Situ Growth of Monodisperse Fe_3O_4 Nanoparticles on Graphene as Flexible Paper for Supercapacitor. *J. Mater. Chem. A* **2014**, *2*, 12068−12074.
(34) Wang, H.; Sun, K.; Tao, F.; Stacchiola, D. J.; Hu, Y. H. 3D Honeycomb-Like Structured Graphene and Its High Efficiency as a Counter-Electrode Catalyst for Dye-Sensitized Solar Cells. *Angew. Chem., Int. Ed.* **2013**, *52*, 9210−9214.
(35) Hu, W. B.; Peng, C.; Luo, W. J.; Lv, M.; Li, X. M.; Li, D.; Huang, Q.; Fan, C. H. Graphene-Based Antibacterial Paper. *ACS Nano* **2010**, *4*, 4317−4323.
(36) Akhavan, O.; Ghaderi, E. Toxicity of Graphene and Graphene Oxide Nanowalls Against Bacteria. *ACS Nano* **2010**, *4*, 5731−5736.
(37) Musico, F.; Santos, C. M.; Dalida, M. P.; Rodrigues, D. F. Surface Modification of Membrane Filters Using Graphene and Graphene Oxide-Based Nanomaterials for Bacterial Inactivation and Removal. *ACS Sustainable Chem. Eng.* **2014**, *2*, 1559−1565.
(38) Tu, Y. S.; Lv, M.; Xiu, P.; Huynh, T.; Zhang, M.; Castelli, M.; Liu, Z. R.; Huang, Q.; Fan, C. H.; Fang, H. P.; Zhou, R. H. Destructive Extraction of Phospholipids from Escherichia coli Membranes by Graphene Nanosheets. *Nat. Nanotechnol.* **2013**, *8*, 594−601.
(39) Wang, J.; Chen, Z.; Chen, B. Adsorption of Polycyclic Aromatic Hydrocarbons by Graphene and Graphene Oxide Nanosheets. *Environ. Sci. Technol.* **2014**, *48*, 4817−4825.
(40) Wu, Q.; Feng, C.; Wang, C.; Wang, Z. A Facile One-Pot Solvothermal Method to Produce Superparamagnetic Graphene-Fe_3O_4 Nanocomposite and Its Application in the Removal of Dye from Aqueous Solution. *Colloids Surf., B* **2013**, *101*, 210−214.
(41) Feng, B. Y.; Guo, L. J.; Wang, L. H.; Li, F.; Lu, J. X.; Gao, J. M.; Fan, C. H.; Huang, Q. A Graphene Oxide-Based Fluorescent Biosensor for the Analysis of Peptide-Receptor Interactions and Imaging in Somatostatin Receptor Subtype 2 Overexpressed Tumor Cells. *Anal. Chem.* **2013**, *85*, 7732−7737.
(42) Tang, J.; Chen, Q.; Xu, L. G.; Zhang, S.; Feng, L. Z.; Cheng, L.; Xu, H.; Liu, Z.; Peng, R. Graphene Oxide-Silver Nanocomposite As a Highly Effective Antibacterial Agent with Species-Specific Mechanisms. *ACS Appl. Mater. Interfaces* **2013**, *5*, 3867−3874.

DOI: 10.1021/am508682s
ACS Appl. Mater. Interfaces 2015, 7, 4290−4298